Combustion and Flame 258 (2023) 113091

Contents lists available at ScienceDirect

Combustion and Flame

journal homepage: www.elsevier.com/locate/combustflame

On the flow-facilitated ignition in a mixture with low Lewis number

Xinyi Chen[a,b], Hannes Böttler[a], Shumeng Xie[b], Arne Scholtissek[a], Wang Han[a], Christian Hasse[a], Zheng Chen[b,*]

[a] Institute for Simulation of reactive Thermo-Fluid Systems, TU Darmstadt, Otto-Berndt-Straße 2, 64287 Darmstadt, Germany
[b] SKLTCS, CAPT, College of Engineering, Peking University, Beijing 100871, China

ARTICLE INFO

Article history:
Received 3 January 2023
Revised 15 September 2023
Accepted 16 September 2023

Keywords:
Ignition
Lewis number
Critical ignition radius
Heat loss
Hydrogen

ABSTRACT

The imposed laminar flow has been shown to facilitate ignition under certain conditions in our previous work (Chen et al. 2023). Such flow-facilitated ignition (FFI) was observed only for mixtures with sufficiently large effective Lewis numbers, i.e., $Le>>1$. It is not clear whether FFI can also occur in a mixture with $Le<1$ and $Le\sim1$. This study will investigate the occurrence of FFI in a mixture with low Lewis number. We conduct multi-dimensional simulations of forced ignition by a pair of electrodes in both static and flowing hydrogen/air mixtures. A simplified ignition model is used in simulations. The laminar flow direction is perpendicular to the pair of electrodes. We consider different values for equivalence ratio (ϕ=0.4 and 1.0), pressure (P = 0.3–1 atm), electrode gap distance (d_{gap}=0.64–3.88 mm) and flow velocity (U_{in}=0–10 m/s). The simulation results show that FFI can occur in a fuel-lean (ϕ=0.4) H_2/air mixture with $Le\approx0.43$ at sub-atmospheric pressure. This indicates that large Lewis number is not a necessary condition for FFI occurring in simulations considering a simplified ignition model. Here, the favorable conditions for FFI are large critical ignition radius at sub-atmospheric pressure, sufficiently small electrode gap distance and moderate flow velocity. Moreover, the reduction in heat loss to the electrodes by the imposed flow is found to be crucial for FFI. To further understand the boundary conditions of FFI, an ignition mode regime diagram in terms of flow velocity and normalized critical ignition radius (i.e. the ratio of critical ignition radius and electrode gap distance) is proposed. The present study provides insights on the effects of laminar flow on forced ignition of premixed flames.

1. Introduction

Contrary to the belief that turbulence suppresses ignition due to the enhanced heat loss from the ignition kernel to the surroundings, turbulence-facilitated ignition (TFI) has been observed by Law and his co-workers [1] in a fuel-rich (ϕ=5.1) hydrogen/air mixture with an effective Lewis number of $Le\approx2.3$. TFI was attributed to the fact that turbulence breaks the single, highly positively stretched, ignition kernel into a multitude of wrinkled flame elements with both positive and negative stretch, such that the intensified burning of the flame segments with negative stretch at $Le>1$ helps to promote ignition [1]. Such facilitating effects have been confirmed by many experiments [1–5], showing that TFI occurring in mixtures with large Le is indeed a general behavior, irrespective of fuel, equivalence ratio, and inert dilution. Recently, Shy and coworkers [2,3,5] assessed the effects of electrode gap distance on ignition kernel development and found that TFI occurs only for mixtures with sufficiently large Lewis number ($Le>>1$) and small gap distance (d_{gap} typically less than 1 mm [6]). In these studies, both heat loss to electrodes and differential diffusion were found to be important for the occurrence of TFI. It was argued that a flame kernel might be easier to survive when it moves with the turbulent wind away from the spark gap [2]. Furthermore, TFI has not been observed in experiments for mixtures with $Le<1$ [1–5] and $Le\sim1$ [1]. A more detailed description of the developments on premixed turbulent spark ignition can be found in a recent review paper by Shy [6].

While TFI has been widely observed in previous experiments, it has not been reproduced in simulations yet. Uranakara et al. [7] conducted DNS of forced ignition in a turbulent H_2/air mixture with ϕ=4 and $Le\approx2.15$ but did not observe TFI. They showed that turbulence locally wrinkles the flame front into more positively stretched structures, as such renders ignition at $Le>1$ more difficult. In the simulations by Uranakara et al. [7], a hot spot was used to ignite the mixture. The electrodes and the heat loss to them were not considered, which is one potential reason for not observing TFI. In our recent simulations [8], we considered the existence of electrodes in the forced ignition of a fuel-rich (ϕ=5.1) H_2/air mixture with $Le\approx2.3$ without an imposed turbulent

* Corresponding author.
E-mail address: cz@pku.edu.cn (Z. Chen).

https://doi.org/10.1016/j.combustflame.2023.113091
0010-2180/

flow. A uniform inlet laminar flow was used to mimic the local turbulent flow around the electrodes which blows the ignition kernel away from the electrodes. The flow-facilitated ignition (FFI) phenomenon was observed [8]. Similar to TFI, FFI was observed for large Lewis number of $Le\approx2.3$ and sufficiently small electrode gap of d_{gap}=0.64 mm. Since FFI has some similarities with TFI, the above study [8] is one important step to identify the underlying mechanisms for TFI observed in experiments [1–5].

As mentioned above, in previous works both TFI and FFI were observed only for sufficiently large Lewis number, and differential diffusion was considered to be crucial. The requirement of $Le>>1$ was proposed to be one of the necessary conditions for TFI [4]. Currently, it is not clear whether FFI can occur in a mixture with $Le< 1$ and $Le\sim1$. This motivates the present study, which explores whether the interesting FFI phenomenon can occur for a mixture with $Le<1$ and $Le\sim1$.

The premixed flame initiation process is complex, as recently reviewed by Shy [6]. For simplicity, the present simulations do not consider the breakdown process and the emitted shock wave in the very early stage; we focus on the following two phases: (1) thermal runaway and formation of an ignition kernel and (2) transition of the ignition kernel into a self-sustained propagating flame [9]. The first phase requires the maximum temperature to be high enough to trigger thermal runaway and to ensure that chemical heat generation is faster than heat loss [10]. The second phase requires the flame kernel to reach the critical ignition radius, which is mainly determined by the effective Lewis number and flame thickness of the mixture [11,12]. As shown in [8], the imposed flow has both facilitating and inhibiting effects on the ignition kernel evolution. The inhibiting effect originates from the convective dissipation of the deposited energy which suppresses thermal runaway, while the facilitating effect is due to the reduction in both the heat loss to electrodes and flame curvature/stretch during the ignition kernel transition stage. Therefore, FFI is expected to occur when it is difficult for the ignition kernel to reach the critical ignition radius and to evolve into an expanding flame. This scenario is of a general nature irrespective of the Lewis number. For instance, at lower/higher pressure the flame thickness becomes larger/smaller and so does the critical ignition radius [13]. Consequently, premixed flame ignition is extremely difficult at reduced pressure even for a mixture with low Lewis number. Therefore, here we consider ignition of a lean H_2/air mixture at lower pressures with $Le<1$ and $Le\sim1$. The first objective is to demonstrate that FFI can occur even in a mixture with $Le<1$ and $Le\sim1$ in simulations considering a simplified ignition model. Moreover, the imposed flow has a dissipative effect on the deposited energy. Therefore, the second objective of this study is to investigate the dependence of forced ignition on the flow velocity and to explore the possible upper bound for the FFI. Note that the present study considers the laminar flame instead of turbulent flow. The effects of turbulence on ignition are beyond the scope of the present study and need to be explored in future studies. Besides, here a simplified ignition model is considered in simulations, and it is not the same as practical ignition process.

2. Model and numerical methods

Similar to our previous study [8], we consider the forced ignition induced by a pair of fixed electrodes in an initially quiescent or flowing H_2/air mixture at T_0=298 K and P = 0.3–1 atm. The simulations are extended to cover different Lewis numbers, especially focusing on mixtures with $Le<1$ and $Le\sim1$, such that ignition evolution is not limited by the large positive stretch. Specifically, we consider two H_2/air mixtures with ϕ=0.4 ($Le\approx0.43$) and ϕ=1.0 ($Le\approx1.05$) [14]. For the quiescent mixture, the configuration is axisymmetric along the center line of the electrodes (see Fig. 1a), and

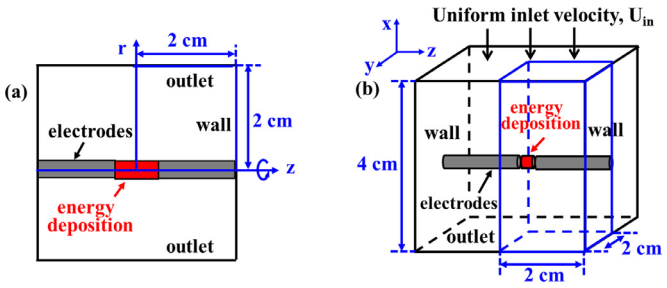

Fig. 1. Schematics of the (a) 2D and (b) 3D simulation setup. The blue rectangle and cuboid represent the computational domains in the 2D and 3D simulations, respectively.

thereby 2D simulations are conducted. For the case with imposed laminar flow, the flow is oriented perpendicular to the electrodes (see Fig. 1b) and thereby 3D simulations are performed. Gravity is not considered in the simulations. Therefore, due to symmetry, the computational domain is a quarter of the whole region shown in Fig. 1, in which the boundary conditions as well as the dimensions are also depicted. For the case with imposed flow, a uniform inlet velocity, U_{in}, is prescribed at the top boundary (see Fig. 1b), and the steady cold flow field is used as the initial velocity field for the subsequent reactive flow simulations. Compared to our previous study, a larger magnitude of inlet velocities in the range of U_{in}=0–10 m/s is studied to explore possible occurrence of FFI.

For simplicity, the electrical energy discharge process (e.g. the plasma formation, shock wave) is not considered in the simulations. We undertake a well-controlled numerical approach to mimic the spark ignition process in experiments. As shown in the red region of Fig. 1, the ignition energy is released uniformly in the cylindrical space between the two electrodes at a constant ignition energy density, q_{ig}, during the spark duration τ_{ig}. The ignition energy is:

$$E_{ig} = \pi R_e^2 d_{gap} \tau_{ig} q_{ig}, \tag{1}$$

where R_e is the radius of the electrodes and d_{gap} is the gap spacing between them. Here, we fix τ_{ig}=0.2 ms and R_e=0.32 mm. A wide range of gap distances, d_{gap}=0.64–3.84 mm is chosen to assess the effects of the electrode gap on the ignition kernel evolution. At a specified ignition energy, the energy density, q_{ig}, can be evaluated according to Eq. (1) and it is included in the energy equation as a source term in all simulations. The electrode surface is modeled as inert non-slip wall with fixed surface temperature, T_s=298 K. As demonstrated in [8], assuming a constant wall temperature is valid due to the high heat capacity of the electrodes and the short ignition time. It is noted again that the simplified ignition model described above cannot represent stochastic nature of the electric spark breaking down and flame kernel onset occurring in practical spark ignition processes. Consequently, the statistical nature of MIE measured in experiments (see [6] and references therein) cannot be captured in the present simulations.

2D and 3D simulations of the transient ignition process are conducted using an OpenFOAM-based solver developed by Zirwes et al. [15,16]. The finite volume method is used to solve the compressible conservation equations for multi-component reactive flows. The detailed chemistry for hydrogen developed by Li et al. [17] is used. Cantera [18] is incorporated to calculate the reaction rates as well as transport coefficients. The mixture-averaged model is used to evaluate the mass diffusivities for all species. This code has been successfully used in recent studies on premixed flames [19–22]. More details on the numerical schemes and the code validation can be found in [15,16]. In all simulations, a non-uniform mesh is adopted and the size of the smallest cell is 16 μm. During the ignition kernel development, the reaction front is always

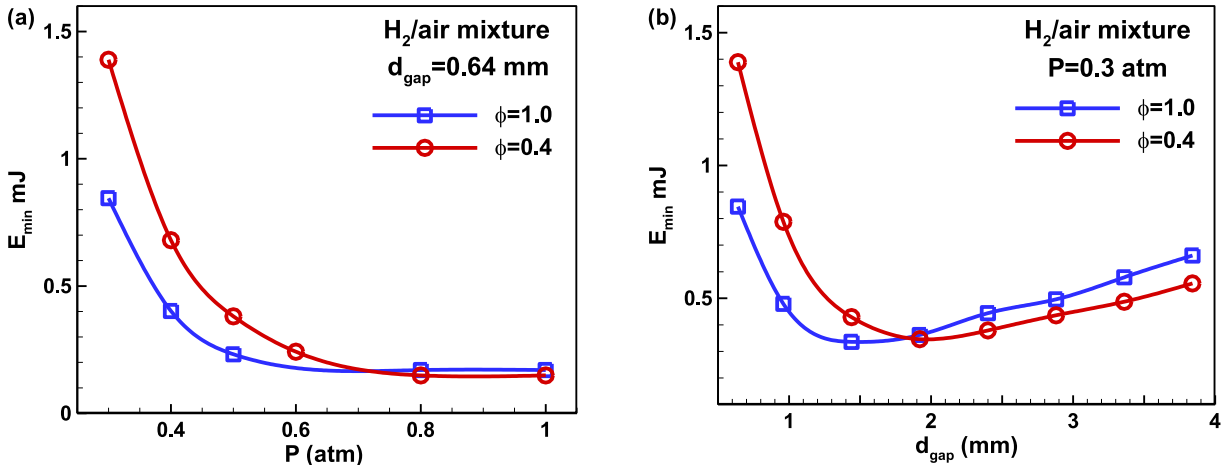

Fig. 2. Change of the MIE with (a) pressure and (b) electrode gap distance for quiescent fuel-lean (ϕ=0.4) and stoichiometric (ϕ=1) H_2/air mixtures.

resolved by more than 30 grid points so that grid convergence is ensured.

3. Ignition in quiescent mixtures at reduced pressures

We first consider forced ignition for the two H_2/air mixtures at quiescent conditions. In order to quantify the effects of pressure and electrode gap distance on forced ignition. The minimum ignition energies (MIE) are calculated for a wide range of pressure (i.e. P = 0.3–1 atm) and electrode gap distance (d_{gap}=0.64–3.88 mm) in fuel-lean (ϕ=0.4) and stoichiometric (ϕ=1) H_2/air mixtures. The results are shown in Fig. 2.

Figure 2(a) shows that for both fuel-lean and stoichiometric H_2/air mixtures, MIE significantly increases with decreasing pressure. The MIE at P = 0.3 atm is about nine and five times of that at P = 1 atm for ϕ=0.4 and ϕ=1, respectively. Compared to the stoichiometric case, the MIE is more sensitive to a pressure change in the fuel-lean case. Existing studies have demonstrated that the flame thickness becomes larger at lower pressures and so does the critical ignition radius [13,23]. Therefore, it is more difficult to achieve successful ignition at a lower pressure, so a higher MIE is required.

Figure 2(b) shows the effect of electrode gap distance on MIE at P = 0.3 atm. It is observed that for ϕ=0.4 the MIE is lowest at d_{gap} =1.92 mm, and that the MIE decreases drastically from 1.39 mJ to 0.35 mJ in the range of d_{gap} =0.64–1.92 mm. For d_{gap} ≥1.92 mm, the MIE increases slightly with d_{gap}. A similar trend is also observed for the stoichiometric case. As introduced by Lewis and von Elbe [24], there exists a quenching distance d_q which is related to the critical ignition radius in the classic thermal-diffusion theory. When $d_{gap}<<d_q$, the initial ignition kernel suffers significant heat loss to the electrodes, making it difficult to reach successful ignition unless a sufficiently large ignition energy is applied to overcome the associated heat loss. Besides the heat loss to the electrodes, differential diffusion (i.e., Lewis number effect) is also responsible for the large MIE at small d_{gap} when $Le>>1$ [3,5,8]. By decreasing d_{gap}, the initial ignition kernel transforms from a rod-like shape with small or negligible curvature/stretch to a ball-like shape with high curvature/stretch [3,5,8]. Therefore, a higher MIE at a small d_{gap} is required to overcome the incipient extinction by larger positive curvature stretch due to the weakening effect of differential diffusion for $Le>>1$. For the present fuel-lean and stoichiometric H_2/air mixture, the effective Lewis number is lower than unity or around unity. Therefore, the flame kernel is strengthened by positive stretch rate at smaller d_{gap}. However, when $d_{gap}<d_q$, the heat loss to electrodes plays dominant role and thereby the MIE decreases with increasing d_{gap}. When $d_{gap}>d_q$, the heat loss to the electrodes is less relevant or even becomes negligible. Thus, the MIE remains nearly constant over a broad range of d_{gap}. This was confirmed by both experiments [5] and detailed chemical kinetics of numerical simulations [25]. The MIE curve in Fig. 2(b) is similar to that of Fig. 11 in [25]. Therefore, it is estimated that d_q is around 1.92 mm and 1.44 mm respectively for ϕ=0.4 and ϕ=1. In summary, Fig. 2 shows that successful forced ignition is extremely difficult at a reduced pressure and a small electrode gap distance for both fuel-lean and stoichiometric H_2/air mixtures. In the following analysis, a fuel-lean H_2/air mixture with ϕ=0.4 is selected as the reference case for further analysis.

Figure 3 shows the effects of pressure and electrode gap distance on the temporal evolution of the maximum temperature during the ignition of a H_2/air mixture with ϕ=0.4. The solid and dashed lines represent the evolution of the maximum temperature during the successful and failed ignition process close to critical conditions, respectively (i.e. a small difference in deposited energy). As shown in Fig. 3(a), at P = 1atm the MIE is mainly determined by the thermal runaway phase. Ignition fails when the maximum temperature is not high enough to trigger thermal runaway. Therefore, a relatively low MIE of E_{min}=0.149 mJ is required at P = 1atm. At P = 0.3 atm, the MIE increases to E_{min}=1.389 mJ and Fig. 3(a) shows that the maximum temperature of the ignition kernel is quite high at t = 0.2 ms. Therefore, thermal runaway readily occurs during the energy deposition. However, the ignition can still fail when the flame kernel cannot transition into a self-sustained flame (see the red dashed line in Fig. 3a). Therefore, ignition is mainly determined by the flame kernel transition phase. Based on the dominant ignition phase, we can identify two ignition modes: thermal runaway dominated mode (mode I) and ignition kernel propagation dominated mode (mode II). Fig. 3(b) shows that ignition is mainly dominated by the thermal runaway phase at large d_{gap}, and by ignition kernel propagation phase at a small d_{gap}. Therefore, Fig. 3 shows that both decreasing the pressure and decreasing the electrode gap distance can result in the transition from ignition mode I to ignition mode II. According to our previous study [8], FFI usually occurs for ignition mode II. Therefore, it is expected that FFI occurs at reduced pressure and small electrode gap distance.

Based on these findings, the effect of ignition energy, E_{ig}, on the evolution of the flame displacement speed, S_d is shown in Fig. 4(a) for ϕ=0.4, P = 0.3 atm and d_{gap}=0.64 mm. In the simulations, the flame radius, R_f, is defined at the location of the flame front in the radial direction (i.e. z = 0). The displacement speed is based on the

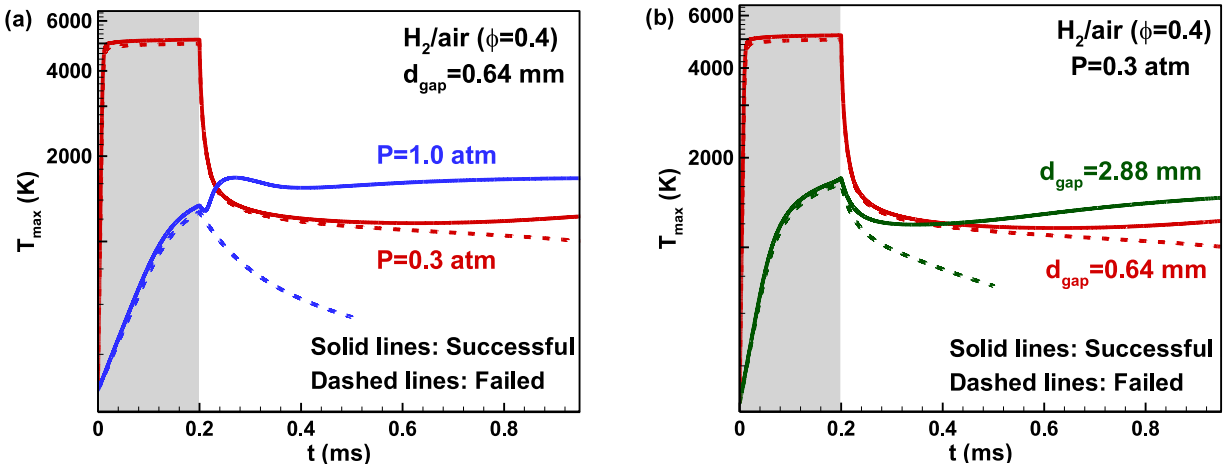

Fig. 3. Effects of (a) pressure and (b) electrode gap distance on the ignition process of a quiescent H_2/air mixture with ϕ=0.4. The solid and dashed lines represent the evolution of the maximum temperature during the successful and failed ignition process close to critical conditions, respectively. The shaded region marks the duration of energy deposition.

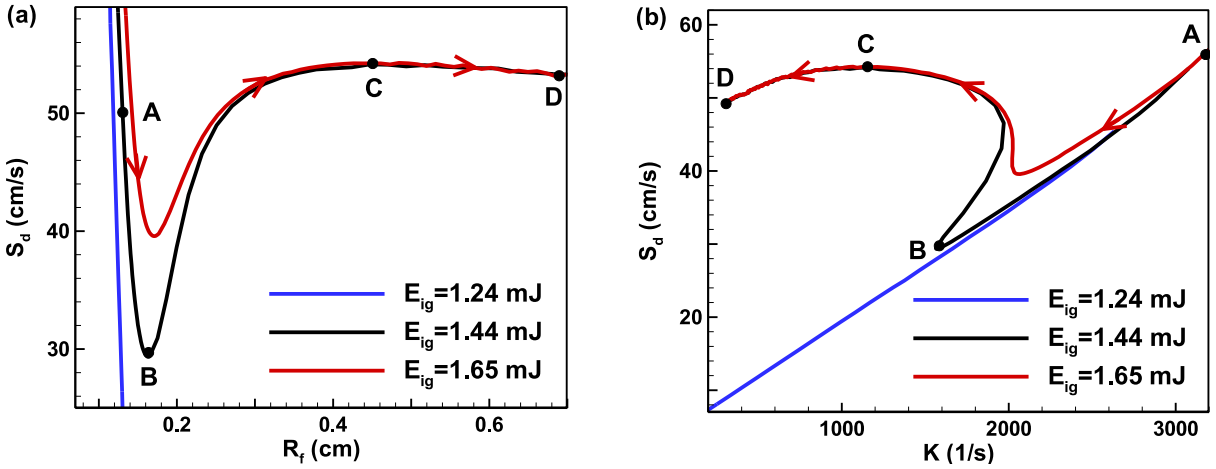

Fig. 4. Change of flame displacement speed with (a) flame radius and (b) stretch rate for a quiescent H_2/air mixture with ϕ=0.4, P = 0.3 atm and d_{gap}=0.64 mm.

isosurface of H_2O mass fraction and it is defined as [26]:

$$S_d = -\left[\frac{\omega_{H_2O}}{\rho_u\left|\nabla Y_{H_2O}\right|} + \frac{\nabla\cdot\left(\rho D_{H_2O}\nabla Y_{H_2O}\right)}{\rho_u\left|\nabla Y_{H_2O}\right|}\right] \quad (2)$$

where ρ is the density, ρ_u is the density of unburnt mixture, ω_{H2O} is the production rate of H_2O, and D_{H2O} is the mass diffusion coefficient of H_2O. The representative isosurface of Y_{H2O} = 0.0618 is chosen since its position is close to that of the local maximum heat release rate in the unstretched laminar planar flame. The MIE for this mixture is E_{min} =1.44 mJ and ignition fails for $E_{ig}<E_{min}$. Similar to previous studies [27,28], Fig. 4(a) indicates that there exist three distinct flame regimes for the successful ignition case: the spark-assisted ignition kernel propagation regime (AB), the unsteady flame transition regime (BC), and the quasi-steady flame propagation regime (CD). These three regimes are more clearly demonstrated in Fig. 4(b), which plots S_d as a function of the local stretch rate, K. Usually these regimes are observed for mixtures with $Le>1$ where ignition is limited by the difficulty of the flame kernel to transition into an expanding flame (i.e. ignition mode II). However, Fig. 4 shows that even for $Le<1$ flames, different regimes are observed and there exists a critical ignition radius (i.e. R_f at point B) at reduced pressure and small d_{gap}. Therefore, ignition mode II is not constrained by Lewis number and it can happen in a mixture with $Le<1$ when the critical ignition radius is large (e.g., at low pressure). This helps to make FFI to occur in a mixture with $Le<1$ as shown in the following section.

Table 1
Ignition cases in static and flowing H_2/air mixture.

Case	ϕ	P (atm)	d_{gap} (mm)	E_{ig} (mJ)	U_{in} (m/s)
A	0.4	0.3	0.64	1.24	0
B	0.4	0.3	0.64	1.24	6
C	0.4	0.3	0.64	1.24	10
D	0.4	0.3	1.44	0.37	0
E	0.4	0.3	1.44	0.37	6
F	0.4	0.3	1.44	0.37	10

4. Ignition in mixtures with imposed flow at reduced pressures

In this section, we consider a uniform flow at the inlet (see Fig. 1b) and assess the effect of flow around the electrodes on forced ignition. Figure 5 compares the ignition kernel evolution in quiescent (U_{in}=0 m/s) and flowing (U_{in}=6 and 10 m/s) H_2/air mixture for Cases A-C (d_{gap}=0.64 mm) and D-F (d_{gap}=1.44 mm), as listed in Table 1. Note that although a relatively large electrode gap distance is considered in Cases D-F, we still have d_{gap}=1.44 mm$<d_q\approx$1.92 mm, which indicates that the heat loss to electrodes is still very important in this case. The evolution of the maximum temperature is compared in Fig. 6.

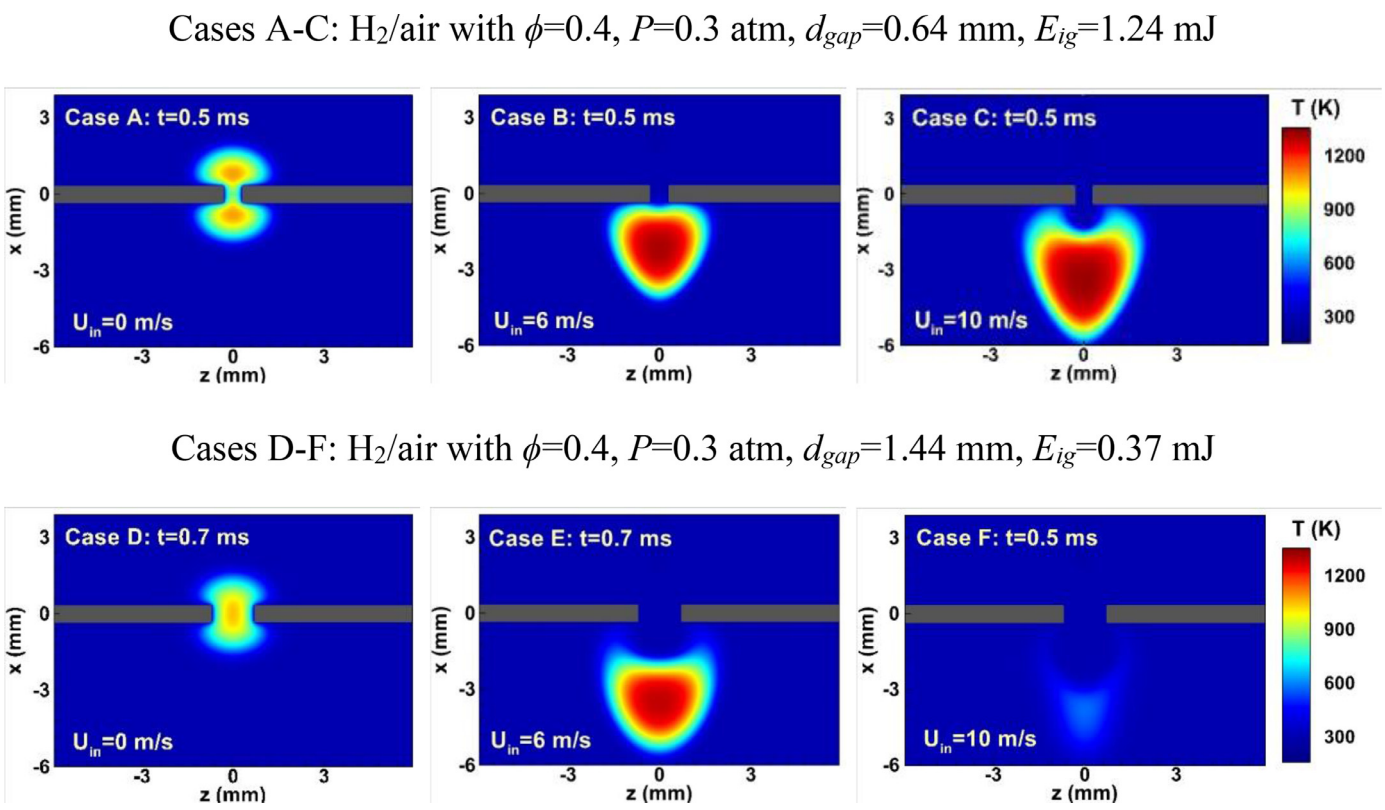

Fig. 5. Comparison of the temperature contours on the plane at $y = 0$ mm during ignition for Cases A-F.

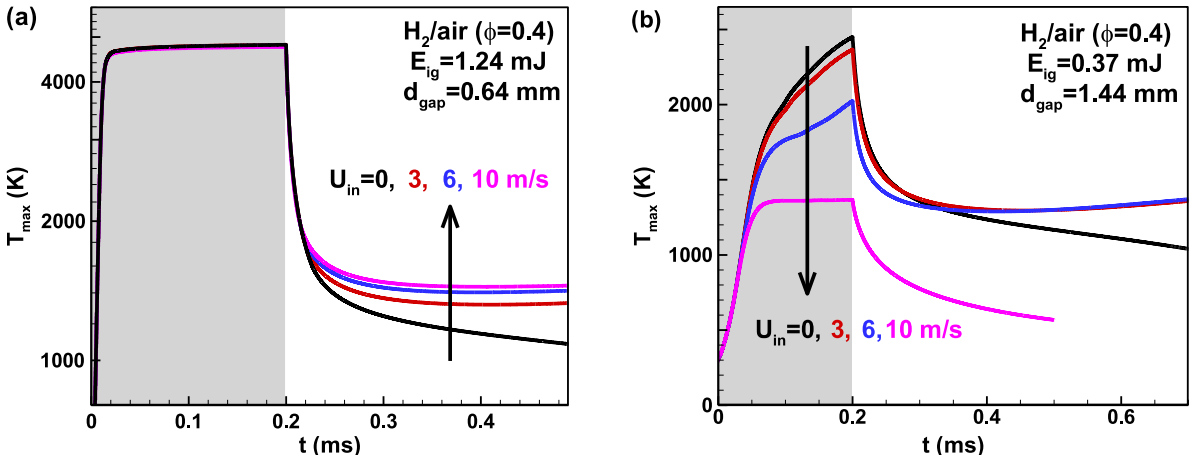

Fig. 6. Evolution of maximum temperature along the line $y = z = 0$ mm during the ignition kernel development in quiescent and flowing H_2/air mixture for (a) Cases A-C: d_{gap}=0.64 mm, E_{ig}=1.24 mJ and (b) Case D-F: d_{gap}=1.44 mm, E_{ig}=0.37 mJ. The shaded region marks the duration of energy deposition.

Figs. 5 (top row) and 6(a) show that at a small electrode gap distance of d_{gap}=0.64 mm, the MIE for U_{in}=6 m/s is lower than that for U_{in}=0 m/s, indicating the occurrence of FFI in simulations. When the inlet velocity is further increased to U_{in}=10 m/s, the facilitating effect is even more evident. At a relatively large electrode gap distance of d_{gap}=1.44 mm (cf. Cases D-F in Fig. 5, bottom row), the non-monotonic transition from ignition failure (i.e. at U_{in}=0 m/s), to successful ignition (i.e. at U_{in}=6 m/s), and to ignition failure (i.e. at U_{in}=10 m/s) again with increasing inlet velocity is observed. Note that Fig. 5 only shows the results on the plane at $y = 0$ mm. The 3D ignition kernel evolution for Cases D-F is shown in Fig. 7, which show the full complexity of the flow effect.

The above simulation results demonstrate that FFI can occur in a mixture with Le<1 at reduced pressure and small d_{gap}, and that there exists an upper limit of inlet velocity beyond which FFI cannot happen. This upper limit of inlet velocity becomes larger at a smaller d_{gap}. Then, we shall address the following questions: what are the reasons for the occurrence of FFI in a mixture with low Lewis number? What are the reasons for the non-monotonic effect of flow on the ignition process? How does this non-monotonic behavior vary with a change of electrode gap distance?

4.1. Effects of inlet flow on flame dynamics

In our previous study [8] we showed that the heat loss to electrodes has both thermal and kinetic effects on the ignition kernel development. Thermal suppression is achieved by decreasing the temperature of the ignition kernel via heat conduction from ignition kernel to cold electrodes. Kinetic suppression is accomplished by wrinkling the reaction front of ignition kernel into a more pos-

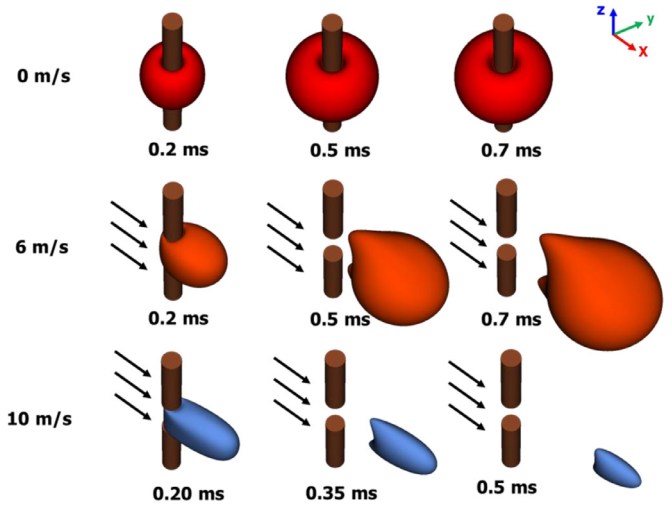

Fig. 7. Evolution of the ignition kernel in quiescent (U_{in}=0 m/s, red) and flowing (U_{in}= 6 m/s, orange and U_{in}=10 m/s, blue) mixtures for Cases D-F (H_2/air with ϕ=0.4, P = 0.3 atm, d_{gap}=1.44 mm, E_{ig}=0.37 mJ).

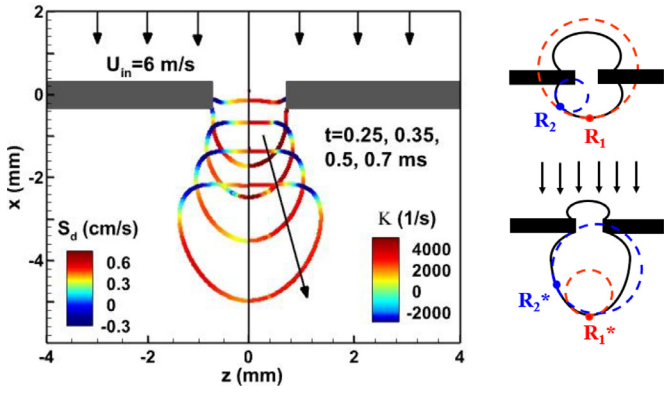

Fig. 8. Evolution of the reaction front (defined with H_2O mass fraction isoline of Y_{H2O} =0.0618) for Case E (H_2/air with ϕ=0.4, P = 0.3 atm, d_{gap}=0.64 mm, E_{ig}=1.24 mJ and U_{in}=6 m/s). The color in the left and right sub-figures represents the magnitudes of displacement speed and stretch rate, respectively. The sketches in the right column schematically show the ignition kernel in quiescent and flowing mixtures.

itively curved structure in close vicinity around the electrodes and thereby increases the global curvature of the ignition kernel. Unlike quiescent mixtures, the imposed flow normal to the electrode blows the flame kernel away from the electrodes and the flame kernel consists of elements with both relatively large curvature (see the red points in the sketches of Fig. 8 where $1/R_1 < 1/R_1{}^*$, the superscript * corresponds to the case with uniform inlet flow) and relatively small curvature (see the blue points where $1/R_2 > 1/R_2{}^*$). Since these variations in curvatures can have distinctively different effects on the local kernel evolution, it is not straightforward to evaluate the overall effect of differential diffusion on the ignition kernel evolution. A similar phenomenon was also observed in premixed turbulent ignition, where turbulence breaks the single, highly positively stretched, ignition kernel into many wrinkled flame elements with both positive and negative stretch [3]. One attempt to explain the overall effect of differential diffusion was made in our previous study [8], where a global curvature was proposed to help to explain the curvature effect. In this approach, an equivalent radius of the ignition kernel is estimated by assuming a spherical volume of hot gas, $V_{Hot} = \frac{4}{3}\pi R_{eq}^3$, then the global curvature of the ignition kernel is determined by $\kappa_{global} = 1/R_{eq}$. Enforcing an inlet flow breaks the symmetry of the ignition kernel and

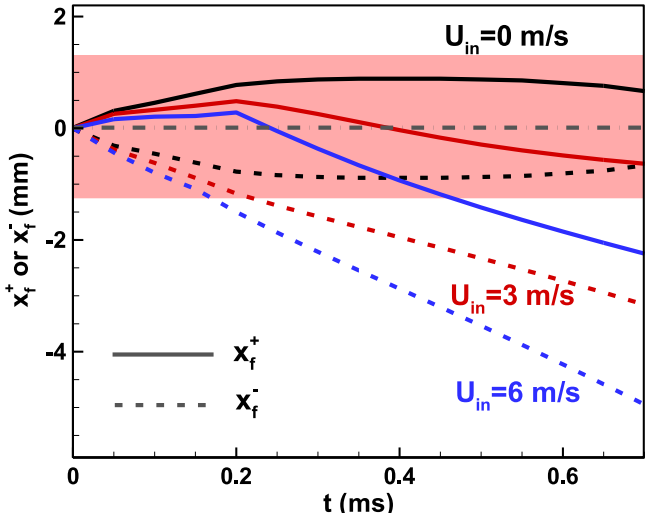

Fig. 9. Evolution of the upstream ($x_f{}^+$) and downstream ($x_f{}^-$) flame position along the line $y = z = 0$ mm during the ignition kernel development for Cases D-E (H_2/air with ϕ=0.4, P = 0.3 atm, d_{gap}=1.44 mm, E_{ig}=0.37 mJ, U_{in}=0, 3, 6 m/s). The gray dashed-dot line represents the position of electrodes and the pink region represents the area within the critical ignition radius (i.e. $x_f < R_c \approx 1.3$ mm).

convectively transports more hot gas to downstream. Therefore, the ignition kernel downstream is modified to a geometry with a larger volume of hot gas and a smaller global curvature, as compared to that in a static mixture (i.e. $V_{Hot} < V_{Hot}^*$ and $\kappa_{global} > \kappa_{global}^*$). This effect becomes more pronounced at a later stage (see the hot gas volumes at t = 0.5 ms in Fig. 5). In [8], the reduction in global curvature was used to explain why the imposed flow can promote ignition in a mixture with Le>1. However, as shown in Fig. 8, for H_2/air mixture with ϕ=0.4 and $Le \approx 0.43$ the displacement speed is now positively correlated with the stretch rate, which indicates that the reduction in curvature/stretch for this Le< 1 mixture is now unfavorable for the flame propagation. Therefore, other effects must be considered to explain the flow facilitated ignition phenomenon observed here for a mixture with a small Lewis number.

To quantify the ignition kernel propagation, we track the positions of flame front upstream and downstream along the line $y = z = 0$ mm, x_f^+ and x_f^- (defined based on the temperature isoline of T = 962 K) and compare the evolution of flame front positions for Cases D-F with U_{in}=0, 3, 6 m/s. The results are shown in Fig. 9. For U_{in}=0 m/s, the flame fronts are symmetric to the electrodes. At E_{ig}=0.37 mJ, the ignition energy is not sufficient to sustain flame propagation. Therefore, the energy is dissipated before x_f^+ or x_f^- has reached the critical flame radius (see the pink region in Fig. 9), finally leading to extinction (x_f^+ and x_f^- will eventually decrease to zero). Maintaining the ignition energy constant but progressively increasing the inlet velocity breaks the symmetry of the ignition kernel (see the schematic on the right hand side of Fig. 8). As shown in Fig. 9, compared to the flame kernel in a quiescent mixture, the flame kernel downstream (i.e. x_f^-) in the flowing environment (see the red and blue lines) has a much larger initial radius. Furthermore, the passage of gas through the discharge region also helps to effectively heat more fresh gasses resulting in a larger volume of "activated mixture" without the need for rapid gas expansion, which further increases the size of the initial kernel downstream. Both effects help the ignition kernel to traverse the critical ignition radius and become self-sustained. This describes one possible scenario of FFI for Le< 1. It is the increase in the initial radius that helps the ignition kernel downstream to survive the flame transition phase and thereby facilitates ignition.

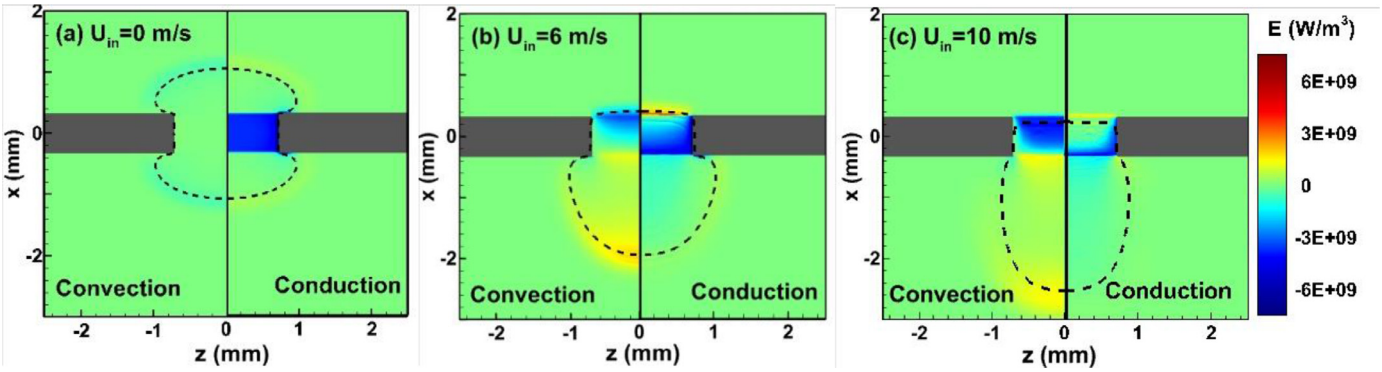

Fig. 10. Contours of convective and conductive terms in energy equation at t = 0.2 ms for Cases D-F with (a) U_{in}=0 m/s, (b) U_{in}=6 m/s and (c) U_{in}=10 m/s.

4.2. Effects of inlet flow on heat transfer

The reduction in heat loss to electrodes by imposed flow was identified to be the main reason for FFI in [8]. It was demonstrated that the imposed flow has both facilitating and dissipative effects on the heat transfer from the ignition kernel. In this subsection, we shall demonstrate that the heat transfer still plays an essential role in FFI observed for Le<1. Therefore, a similar energy budget analysis is conducted to quantify the convective heat loss induced by imposed flow and the conductive heat transfer from the hot ignition kernel to the cold electrodes. The convective and conductive terms in the energy equation are evaluated:

$$E_{Conv} = -\rho C_p u_i \frac{\partial T}{\partial x_i}, \quad E_{Cond} = -\frac{\partial}{\partial x_i}\left(\lambda \frac{\partial T}{\partial x_i}\right) \tag{3}$$

Figure 10 shows the contours of these two terms at the end of the energy deposition, i.e., t = 0.2 ms for Cases D-F: H_2/air with ϕ=0.4, P = 0.3 atm, d_{gap}=1.44 mm, E_{ig}=0.37 mJ and U_{in}=0, 6, 10 m/s. In Fig. 10, the facilitating and dissipative effects are still profound. In a quiescent mixture (i.e. U_{in}=0 m/s), a low convective heat loss is observed within the flame kernel. However, due to the high temperature within the ignition kernel, there is significant conductive heat transfer from the hot gas to the cold electrodes. When the flow is imposed, a strong convective heat transfer is observed from the hot ignition kernel to the unburned mixture downstream (see the left hands of Fig. 10b-c). On one hand, the dissipative effect of the imposed flow lowers the temperature of the ignition kernel (see Fig. 6b), which reduces the available time for chemical reactions to establish an ignition kernel. On the other hand, the inlet flow blows the flame kernel away from the spark gap and thereby reduces the conductive heat loss to electrodes during the ignition kernel propagation (see the right hands of Fig. 10a-c). These two effects are always competing with each other.

At a low velocity level (i.e. U_{in}=6 m/s), the temperature of the ignition kernel is still high. Thermal runaway readily occurs before t = 0.2 ms and the ignition process is mainly dominated by the flame kernel propagation. With the imposed flow, the flame kernel can survive more easily when the heat loss to the cold electrodes is reduced. Therefore, the facilitating effect prevails and FFI can be observed. However, when the inlet velocity is further increased to U_{in}=10 m/s, dissipation of deposited energy kernel is significantly aggravated, chemical reactions cannot be initiated in the first place. In the limit of high flow velocity, the convective dissipation becomes dominant again, constituting an upper ignition boundary.

4.3. Discussion

The above two sub-sections investigate the interactions between flame dynamics, heat transfer, and imposed flow during the forced ignition process. With these results, we can address the questions formulated at the beginning of the section:

What are the reasons for the occurrence of FFI in a mixture with low Lewis number in simulations? The primary reason is that the imposed flow normal to the electrodes tends to blow the flame kernel away from the cold electrodes, reducing the heat loss to the electrodes significantly and modifying the geometry of the flame kernel into a shape with a larger initial radius. Both effects help the embryonic ignition kernel to traverse the critical ignition radius and promote the flame kernel propagation. In [8], the reduction in flame curvature/stretch and the coupling effect between curvature/stretch and Lewis number was used to explain the occurrence of FFI in mixtures with Le>>1. However, differential diffusion effects show an opposing effect for present fuel-lean H_2/air mixtures with Le<1. This indicates that the condition of Le>1 is not necessary in enabling the FFI occurring in simulations. It is the increase in initial radius of the ignition kernel, instead of the reduction in curvature/stretch, that facilitates the ignition kernel propagation in present low pressure case. These results indicate that besides the Lewis number effect, the chemical reactivity of the mixture, which is characterized by the flame thickness, is also essential to the ignition kernel development. Both effects highlight the necessity to incorporate the dynamics of the embryonic ignition structure into the description and prediction of ignition.

What are the reasons for the non-monotonic effect of flow on the ignition process? The imposed flow shows both facilitating and dissipative effects on the heat transfer of the ignition kernel. Irrespective of ignition kernel evolution, flow always increases the dissipation rate of the spark energy and shortens the available time for chemical reactions to establish a self-sustained flame propagation. This dissipative mechanism which suppresses ignition always exists and works against the facilitating mechanism. Therefore, it is expected that the continuous increase in flow velocity will eventually suppress ignition and that there exists an upper limit of flow velocity beyond which such facilitation is not feasible.

How does this non-monotonic behavior vary with a change of electrode gap distance? FFI is expected to occur when ignition is limited by the difficulty of the flame kernel to reach the critical ignition radius and transition into an expanding flame. Decreasing d_{gap} leads to the generation of a small ignition kernel at the very beginning, which increases the heat loss to electrodes and reduces the initial radius of the ignition kernel. Both effects make it more difficult for the ignition kernel to transition into a self-sustained flame. Therefore, it is expected that the window of flow velocity for the facilitated ignition would be larger at smaller $d_{gap.}$ This explains why at the largest available inlet velocity U_{in}=10 m/s, the non-monotonic behavior was observed in Cases D-F (d_{gap}=1.44 mm), while it was not observed in Cases A-C (d_{gap}=0.64 mm). However, it is expected that a continuous increase in flow velocity will eventually

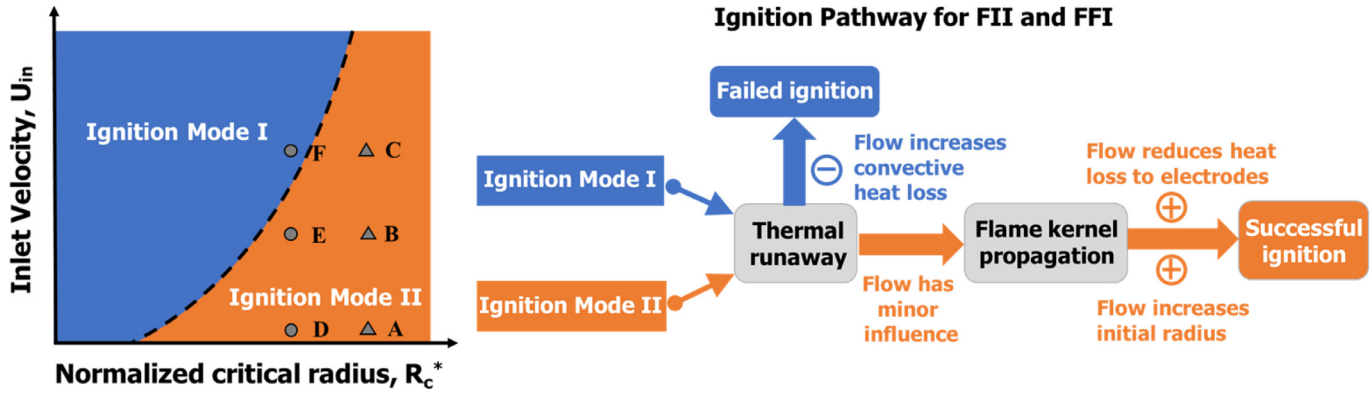

Fig. 11. The regime diagram for ignition mode in the plot of inlet velocity U_{in} versus normalized critical ignition radius R_c^* (which is the ratio of critical ignition radius and electrode gap distance, i.e., $R_c^*=R_c\ /d_{gap}$). The blue and red arrows represent the ignition pathway for flow-inhibited ignition (FII) and flow-facilitated ignition (FFI), respectively. The solid triangles and circles represent the ignition Cases A-C (d_{gap}=0.64 mm) and D-F (d_{gap}=1.44 mm), as listed in Table 1.

still suppress ignition for d_{gap}=0.64 mm, i.e., a non-monotonic influence of imposed flow on spark ignition is still expected.

To summarize the influence of the inlet flow on forced ignition in simulations, we propose a qualitative regime diagram in Fig. 11.

In this study, the coupling effects of heat transfer, flame dynamics, and imposed flow on spark ignition determine two contrary phenomena: flow-inhibited ignition (FII) versus flow-facilitated ignition (FFI). For thermal runaway dominated mode (mode I), flow-inhibited ignition always occurs since the convective heat loss suppresses the occurrence of thermal runaway. However, for the ignition kernel propagation dominated mode (mode II), the imposed flow tends to blow the flame kernel away from the cold electrodes, reducing the heat loss to the electrodes and increasing the initial radius of the flame kernel, leading to FFI.

A qualitative ignition mode regime is extensively mapped out in terms of the inlet velocity and the normalized critical ignition radius (i.e. R_c^*, the ratio of critical ignition radius, R_c and electrode gap distance, d_{gap}), which is shown on the left part of Fig. 11. It is noted that the definition of critical ignition radius concludes both chemical effect (e.g., flame thickness) and *Le* effect during the ignition kernel evolution. Qualitatively, for a quiescent mixture, both increasing R_c and decreasing d_{gap} would result in the ignition transition from mode I to mode II (see Fig. 3). This basically explains why FFI occurs only for mixtures with large Lewis number or reduced pressure (i.e. at large R_c) and small d_{gap}. Similarly, if the inlet velocity is increased at a fixed value of R_c^*, ignition transition from mode II to mode I is achieved by moving vertically across the regime diagram. This is because the dissipative effect of imposed flow decreases the temperature of the ignition kernel. When the temperature is too low, thermal runaway can not be triggered, indicating that the ignition process is now dominated by thermal runaway (mode I). Therefore, flow-inhibited ignition occurs. This transition explains the non-monotonic influence of the imposed flow on forced ignition. It is expected that the crossover velocity between the two ignition mode regimes should increase with increasing R_c^*, as indicated by ignition Cases A-F (see solid symbols in Fig. 11). However, it is difficult to quantify the boundary as an enormous number of simulations would be required. Considering the large computational cost of three-dimensional (3D) DNS, Cases A-C (d_{gap}=0.64 mm) and D-F (d_{gap}=1.44 mm) are judiciously selected to demonstrate a qualitative trend.

In summary, we have presented a comprehensive numerical investigation on the role of imposed flow in ignition kernel development. Such an understanding is of both fundamental relevance and practical significance. For example, ignition at reduced pressure is related to reliable relight at high altitudes in jet-engine design [13] and ignition at sufficiently large Lewis number is crucial to the misfire problems of large hydrocarbons in ultra-lean combustion technology [29,30]. To further explore whether flow-facilitated ignition is a general behavior, additional investigations should be conducted for other mixtures such as NH_3/air (with large flame thickness and low reactivity) and ultra-lean or highly-diluted hydrocarbon/air (with large flame thickness and large Lewis number).

Finally, it should be noted that the FFI reported in this study is only from simulations considering a simplified ignition model. In real experiments, multiple complex effects co-exist and are coupled together, which could possibly affect the occurrence of FFI. For example, the practical ignition process depends on various factors such as flow environment, plasma discharge (i.e. discharge type, discharged current/voltage, pulse duration time), and electrode characteristics (i.e. material, geometry, gap distance) [6,31]. Moreover, as mentioned before the present simplified ignition model cannot represent stochastic nature of practical spark ignition and thereby cannot capture the statistical nature of MIE measured in experiments. In present numerical simulations, the MIE is defined as a threshold value beyond which successful ignition can be obtained; while in experiments, the MIE is commonly defined as the ignition energy at 50% ignitability due to the stochastic nature of ignition [6]. Therefore, the FFI observed in the present simulations may be different from spark ignition in experiments even for the same mixture and the same flow conditions. So far, the FFI still has not been observed in lean hydrogen/air mixture with Le<1 at a low pressure of P = 0.3 atm in experiments (according to personal communication with Prof. Shenqyang (Steven) Shy). The disagreement between simulation and experimental results needs to be explored in future studies.

5. Conclusions

In this study, 2D and 3D simulations are conducted to study the forced ignition of hydrogen/air mixtures with ϕ=0.4 (Le≈0.43) and ϕ=1.0 (Le≈1.05). It is demonstrated that in simulations considering a simplified ignition model, FFI can occur in a mixture with Le<1 and Le∼1 at reduced pressure.

First, the effects of pressure and electrode gap distance on forced ignition are examined for both fuel-lean and stoichiometric H_2/air mixtures. The results show that MIE significantly increases as pressure decreases, which is attributed to the large critical ignition radius at the reduced pressure. Moreover, it is found that there exists a quenching distance, below which the ignition kernel suffers huge heat losses to electrodes and the MIE increases drastically with the decreasing d_{gap}. Therefore, ignition is extremely dif-

ficult at reduced pressure and small d_{gap}. Based on the evolution of maximum temperature during the ignition process, two ignition modes are identified: thermal runaway dominated mode (mode I) and kernel propagation dominated mode (mode II). Decreasing the pressure and decreasing electrode gap distance both induce the ignition transition from ignition mode I to ignition mode II. For ignition cases which are dominated by ignition kernel propagation phase (i.e. ignition mode II), there exists a large critical ignition radius and ignition is limited by the difficulty of the flame kernel to transition into an expanding flame.

Then the effects of flow around the electrodes are assessed via 3D simulations of ignition in a flowing H_2/air mixture. While imposed flow was previously believed to promote ignition for mixtures with $Le>>1$, this study demonstrates that FFI can also occur in a fuel-lean H_2/air mixture with $Le<1$ at reduced pressure and small d_{gap}. The imposed flow blows the flame kernel away from the cold electrodes, reducing the heat loss to the electrodes and modifying the geometry of the flame kernel into a shape with a larger initial radius. Both effects help the early ignition kernel to traverse the critical ignition radius and promote the flame kernel propagation. However, at a higher flow velocity, the dissipative nature of flow becomes dominant again, and eventually suppresses ignition. Therefore, there exists an upper limit of inlet velocity beyond which FFI does not occur. This upper limit of inlet velocity becomes larger at a smaller d_{gap}. These results indicate that large Lewis number is not a prerequisite for FFI. The favorable conditions in enabling FFI are large critical ignition radius, sufficiently small d_{gap} and moderate flow velocity. At larger Lewis number, the FFI is expected to be stronger.

Finally, a qualitative regime diagram, in terms of the flow velocity and the normalized critical ignition radius (i.e. the ratio of critical ignition radius and electrode gap distance) is proposed to describe the two contrary phenomena: flow inhibited ignition versus flow facilitated ignition. It is found that imposed flow usually inhibits ignition for ignition mode I and facilitates ignition for ignition mode II. Increasing the critical ignition radius (e.g. increasing Lewis number, reducing the pressure) or decreasing the electrode gap distance might result in the ignition transition from ignition mode I to ignition mode II, leading to FFI. However, increasing the flow velocity at a fixed critical ignition radius may transition the ignition from ignition mode II back to ignition mode I, flipping the flow influence from facilitating to inhibiting again.

It is noted that the present simulation uses energy deposition to achieve ignition and thereby the ignition model is far away from practical spark ignition process which consists of plasma channel formation and its transition to a flame kernel. Moreover, the present simplified ignition model cannot represent stochastic nature of practical spark ignition and thereby cannot capture the statistical nature of MIE measured in experiments. The FFI observed in the present simulations has not been observed in experiments for the same mixture and the same flow conditions (personal communication with Prof. Shenqyang (Steven) Shy). In future works, it would be interesting to use more practical ignition models (e.g., [32]) to assess the effects of uniform flow on ignition kernel development. Besides hydrogen, other fuels such as ammonia and isooctane may be considered. Furthermore, the laminar flow is considered in present simulations; and the influence of turbulent flow needs to be explored in future studies.

Declaration of Competing Interest

The authors declare that they have no known competing financial interests or personal relationships that could have appeared to influence the work reported in this paper.

Acknowledgments

This work was supported by National Natural Science Foundation of China (nos. 52176096 and 51861135309) and German Research Foundation (no. 411275182). We thank Drs. Thorsten Zirwes, Feichi Zhang, and Prof. Henning Bockhorn at Karlsruhe Institute of Technology, for providing us their code. X.C. and Z.C. thank Dr. Dehai Yu for helpful discussion and suggestion on this work. We also thank Prof. Shenqyang (Steven) Shy for providing us their experimental results and for providing constructive comments which greatly improve this paper.

References

[1] F. Wu, A. Saha, S. Chaudhuri, C.K. Law, Facilitated ignition in turbulence through differential diffusion, Phys. Rev. Lett. 113 (2014) 024503.
[2] S.S. Shy, M.T. Nguyen, S.Y. Huang, C.C. Liu, Is turbulent facilitated ignition through differential diffusion independent of spark gap? Combust. Flame 185 (2017) 1–3.
[3] S.S. Shy, M.T. Nguyen, S.Y. Huang, Effects of electrode spark gap, differential diffusion, and turbulent dissipation on two distinct phenomena: turbulent facilitated ignition versus minimum ignition energy transition, Combust. Flame 205 (2019) 371–377.
[4] A. Saha, S. Yang, C.K. Law, On the competing roles of turbulence and differential diffusion in facilitated ignition, Proc. Combust. Inst. 37 (2019) 2383–2390.
[5] S.S. Shy, Y.C. Liao, Y.R. Chen, S.Y. Huang, Two ignition transition modes at small and large distances between electrodes of a lean primary reference automobile fuel/air mixture at 373K with Lewis number>>1, Combust. Flame 225 (2021) 340–348.
[6] S.S. Shy, Spark ignition transitions in premixed turbulent combustion, Prog. Energy Combust. Sci. 98 (2023) 101099.
[7] H.A. Uranakara, S. Chaudhuri, K.N. Lakshmisha, On the extinction of igniting kernels in near-isotropic turbulence, Proc. Combust. Inst. 36 (2017) 1793–1800.
[8] X. Chen, S. Xie, H. Böttler, A. Scholtissek, W. Han, D. Yu, C. Hasse, Z. Chen, Effects of electrodes and imposed flow on forced ignition in laminar premixed hydrogen/air mixtures with large Lewis number, Proc. Combust. Inst. 39 (2023) 1967–1976.
[9] D. Yu, X. Chen, Z. Chen, Analysis on ignition kernel formation in a quiescent mixture: different characteristic time scales and critical heating powers, Combust. Flame 245 (2022) 112336.
[10] N.N. Semenov, Some Problems of Chemical Kinetics and Reactivity, 1, Elsevier, 2013.
[11] Z. Chen, M.P. Burke, Y. Ju, On the critical flame radius and minimum ignition energy for spherical flame initiation, Proc. Combust. Inst. 33 (2011) 1219–1226.
[12] D. Yu, Z. Chen, Theoretical analysis on the transient ignition of a premixed expanding flame in a quiescent mixture, J. Fluid Mech. 924 (2021) A22.
[13] W. Zhang, X. Gou, Z. Chen, Effects of water vapor dilution on the minimum ignition energy of methane, n-butane and n-decane at normal and reduced pressures, Fuel 187 (2017) 111–116.
[14] X. Chen, H. Böttler, A. Scholtissek, C. Hasse, Z. Chen, Effects of stretch-chemistry interaction on chemical pathways for strained and curved hydrogen/air premixed flames, Combust. Flame 232 (2021) 111532.
[15] T. Zirwes, F. Zhang, J.A. Denev, P. Habisreuther, H. Bockhorn, Automated code generation for maximizing performance of detailed chemistry calculations in OpenFOAM, High Performance Computing in Science and Engineering, 17, Springer International Publishing, Cham (2018), pp. 189–204.
[16] T. Zirwes, F. Zhang, P. Habisreuther, M. Hansinger, H. Bockhorn, M. Pfitzner, D. Trimis, Quasi-DNS dataset of a piloted flame with inhomogeneous inlet conditions, Flow, Turbul. Combust. 104 (2020) 997–1027.
[17] J. Li, Z. Zhao, A. Kazakov, F.L. Dryer, An updated comprehensive kinetic model of hydrogen combustion, Int. J. Chem. Kinet. 36 (2004) 566–575.
[18] D.G. Goodwin, Cantera C++ User's Guide, California Institute of Technology, 2002.
[19] X. Chen, Y. Wang, T. Zirwes, F. Zhang, Z. Chen, Heat release rate markers for highly stretched premixed CH_4/air and CH_4/H_2/air flames, Energy Fuels 35 (2021) 13349–13359.
[20] Y. Wang, H. Zhang, T. Zirwes, F. Zhang, H. Bockhorn, Z. Chen, Ignition of dimethyl ether/air mixtures by hot particles: impact of low temperature chemical reactions, Proc. Combust. Inst. 38 (2021) 2459–2466.
[21] F. Zhang, T. Zirwes, Y. Wang, Z. Chen, H. Bockhorn, D. Trimis, D. Stapf, Dynamics of premixed hydrogen/air flames in unsteady flow, Phys. Fluids 34 (2022) 085121.
[22] X. Wen, T. Zirwes, A. Scholtissek, H. Böttler, F. Zhang, H. Bockhorn, C. Hasse, Flame structure analysis and composition space modeling of thermodiffusively unstable premixed hydrogen flames—Part I: atmospheric pressure, Combust. Flame 238 (2022) 111815.
[23] B.X. Lin, Y. Wu, Z.-b. Zhang, Z. Chen, Multi-channel nanosecond discharge plasma ignition of premixed propane/air under normal and sub-atmospheric pressures, Combust. Flame 182 (2017) 102–113.
[24] B. Lewis, G. Von Elbe, Combustion, Flames and Explosions of Gases, Elsevier, 2012.

[25] J. Han, H. Yamashita, N. Hayashi, Numerical study on the spark ignition characteristics of hydrogen–air mixture using detailed chemical kinetics, Int. J. Hydrogen Energy 36 (2011) 9286–9297.
[26] S. Xie, X. Chen, H. Böttler, A. Scholtissek, C. Hasse, Z. Chen, Forced ignition of a rich hydrogen/air mixture in a laminar counterflow: a computational study, Flow, Turbul. Combust. 110 (2023) 441–456.
[27] X. Chen, W. Peng, P. Gillard, L. Courty, M.L. Sankhe, S. Bernard, Y. Wu, Y. Wang, Z. Chen, Effects of fuel decomposition and stratification on the forced ignition of a static flammable mixture, Combust. Theory Model. 25 (2021) 813–831.
[28] Y. Wang, W. Han, Z. Chen, Effects of fuel stratification on ignition kernel development and minimum ignition energy of n-decane/air mixtures, Proc. Combust. Inst. 37 (2019) 1623–1630.
[29] R.D. Reitz, Directions in internal combustion engine research, Combust. Flame 160 (2013) 1–8.
[30] N. Saito, Y. Minamoto, B. Yenerdag, M. Shimura, M. Tanahashi, Effects of turbulence on ignition of methane–air and n-heptane–air fully premixed mixtures, Combust. Sci. Technol. 190 (2018) 452–470.
[31] J.K. Lefkowitz, T. Ombrello, An exploration of inter-pulse coupling in nanosecond pulsed high frequency discharge ignition, Combust. Flame 180 (2017) 136–147.
[32] M. Castela, B. Fiorina, A. Coussement, O. Gicquel, N. Darabiha, C.O. Laux, Modelling the impact of non-equilibrium discharges on reactive mixtures for simulations of plasma-assisted ignition in turbulent flows, Combust. Flame 166 (2016) 133–147.